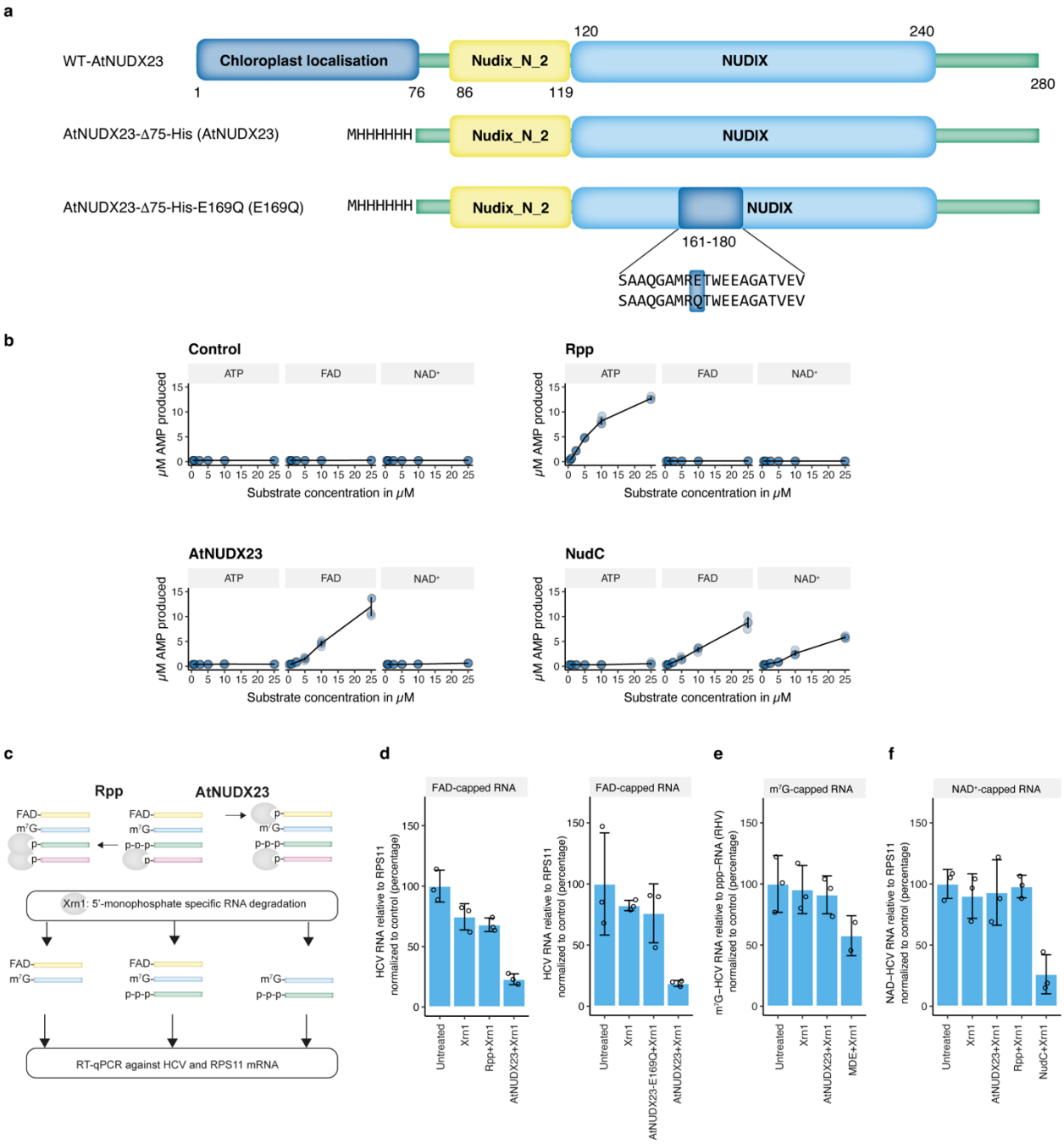

Extended Data Fig.1 | Specificity of enzymes used for CapZyme-seq enrichment
(a) Schematic representation of the AtNUDX23 and AtNUDX23-E169Q proteins used in this study. For both, the N-terminal 75 residues were truncated to remove the chloroplast localisation signal present in the WT protein. **(b)** AMP production in the presence of increasing concentrations of ATP, FAD and NAD^+ for the indicated enzymes and the no enzyme control (n=4, independent replicates). Data are presented as mean +/– SD. **(c)** Strategy for the RT-qPCR reduction assay. **(d)** RT-qPCR reduction assay testing activity of AtNUDX23 and Rpp against *in vitro* transcribed FAD-capped RNA (left) and showing the lack of activity of the AtNUDX23-E169Q protein (right). **(e)** RT-qPCR reduction assay testing activity of AtNUDX23 and mRNA decapping enzyme (MDE) against *in vitro* transcribed m^7G-capped RNA. **(f)** RT-qPCR reduction assay testing activity of AtNUDX23, Rpp and NudC against *in vitro* transcribed NAD^+-capped RNA. For (d-f), data are presented as mean +/– SD, n=3 biological replicates.

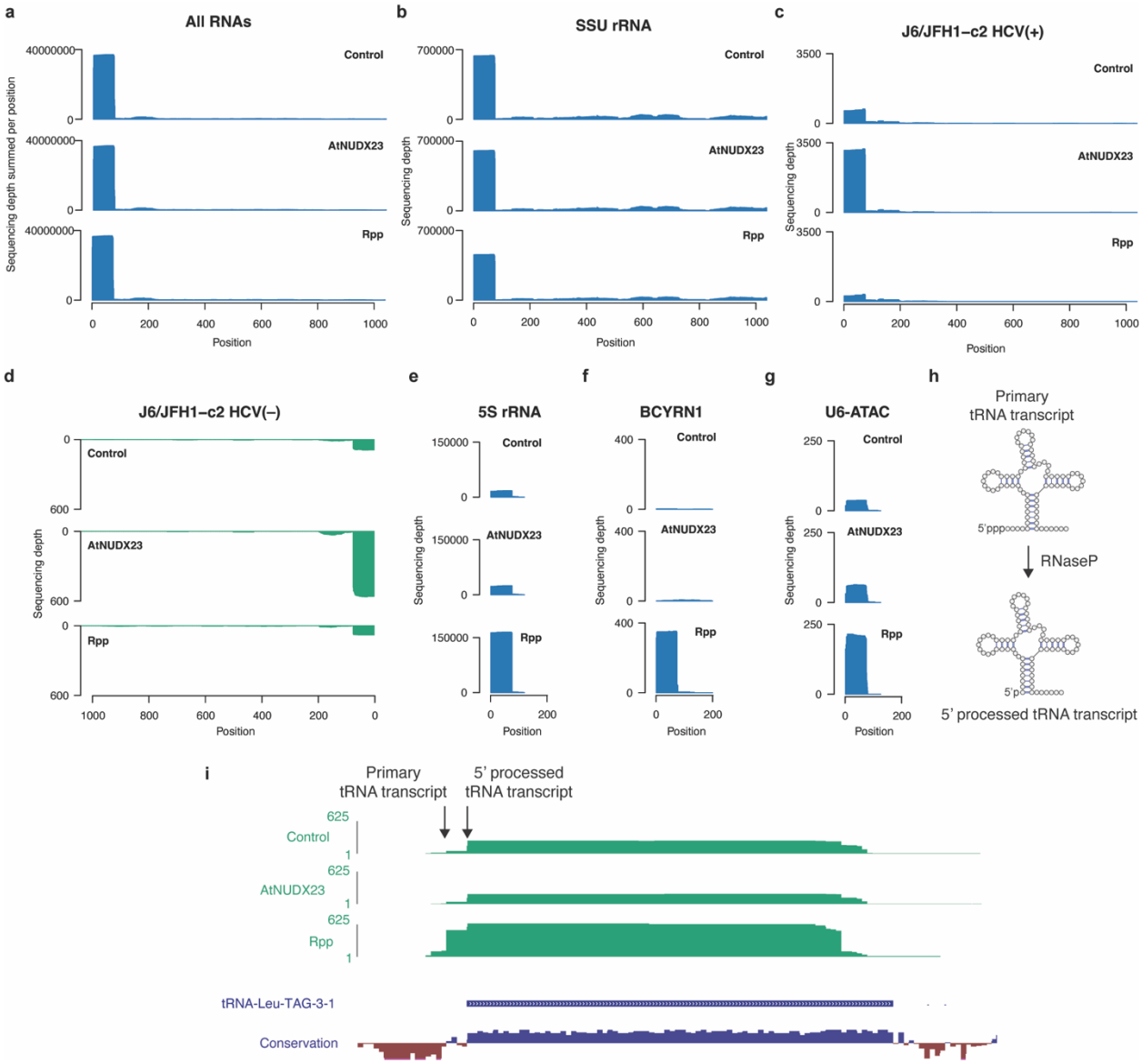

Extended Data Fig.2 | CapZyme-seq reads map to 5' termini of RNAs
Normalized sequencing depth plots for CapZyme-seq libraries: no enzyme control, AtNUDX23 and Rpp enrichment. Reads were mapped to human noncoding RNAs plus the most highly expressed mRNAs (> 2 TPM) in Huh7.5 cells. The normalized sequencing depth is shown for **(a)** all RNAs combined, **(b)** SSU rRNA, **(c)** J6/JFH1-c2 HCV(+) RNA, **(d)** J6/JFH1-c2 HCV(–) RNA, **(e)** 5S rRNA, **(f)** BCYRN1 RNA and **(g)** U6-ATAC RNA. **(h)** Schematic representation of tRNA processing: RNase P mediates processing of 5'ppp termini of primary tRNAs to 5'p mature tRNAs. **(i)** Normalized CapZyme-seq sequencing depth for tRNA-Leu-TAG-3-1 is shown for no enzyme control, AtNUDX23- and Rpp enrichment (top panels). Base wise conservation (phyloP score) for 100 vertebrate species and gene annotation (both obtained from UCSC genome browser) are shown in the bottom panels. Conserved positions have positive phyloP scores (blue). For browsing of the CapZyme-seq data at other human genomic loci the following wiggle files can be uploaded as UCSC custom tracks to the hg19 human genome assembly (http://www.genome.ucsc.edu/cgi-bin/hgCustom?hgsid=1443538613):
http://people.binf.ku.dk/jvinther/data/FAD_Capzyme_seq/Control.wig.gz
http://people.binf.ku.dk/jvinther/data/FAD_Capzyme_seq/Rpp.wig.gz
http://people.binf.ku.dk/jvinther/data/FAD_Capzyme_seq/NUDX23.wig.gz

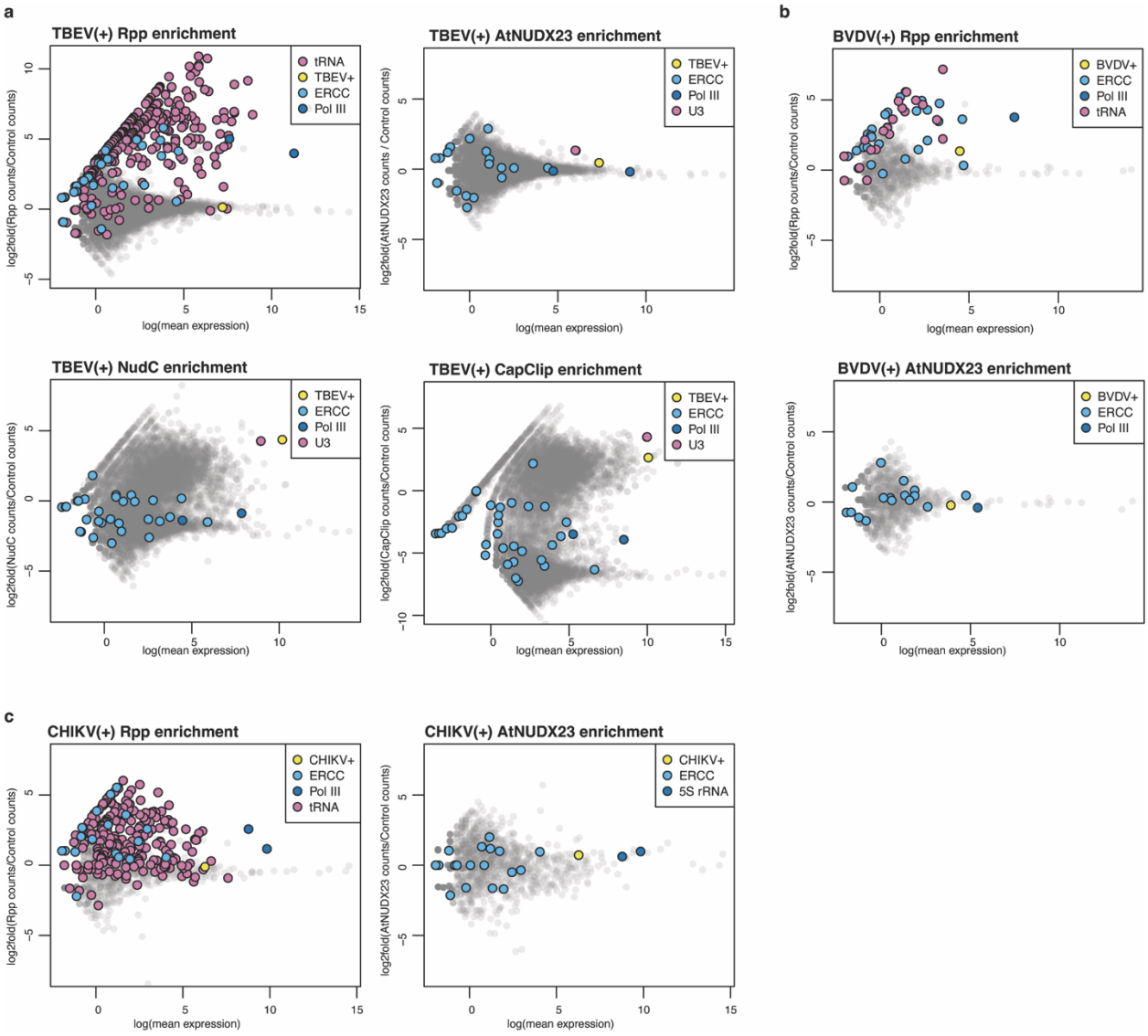

Extended Data Fig.3 | CapZyme-seq analysis of TBEV, BVDV and CHIKV infected cells
Mean-difference plots showing fold changes (log2) as a function of average abundance (log) for reads in 5' termini of individual RNA molecules. **(a)** CapZyme-seq analysis of RNA isolated from SH-SY5Y neuroblastoma cells infected with TBEV using Rpp, AtNUDX23, NudC and CapClip for enrichment. NudC has broad specificity, including cleavage of FAD, NAD^+ and m^7GpppN; Cap-Clip Acid Pyrophosphatase hydrolyzes m^7GpppN (n=3 biological replicates). **(b)** CapZyme-seq analysis of RNA isolated from MDBK bovine kidney cells infected with BVDV using Rpp and AtNUDX23 for enrichment (n=3 biological replicates). **(c)** CapZyme-seq analysis of RNA isolated from TIG3 fibroblast cells infected with CHIKV using Rpp and AtNUDX23 for enrichment (n=2 biological replicates).

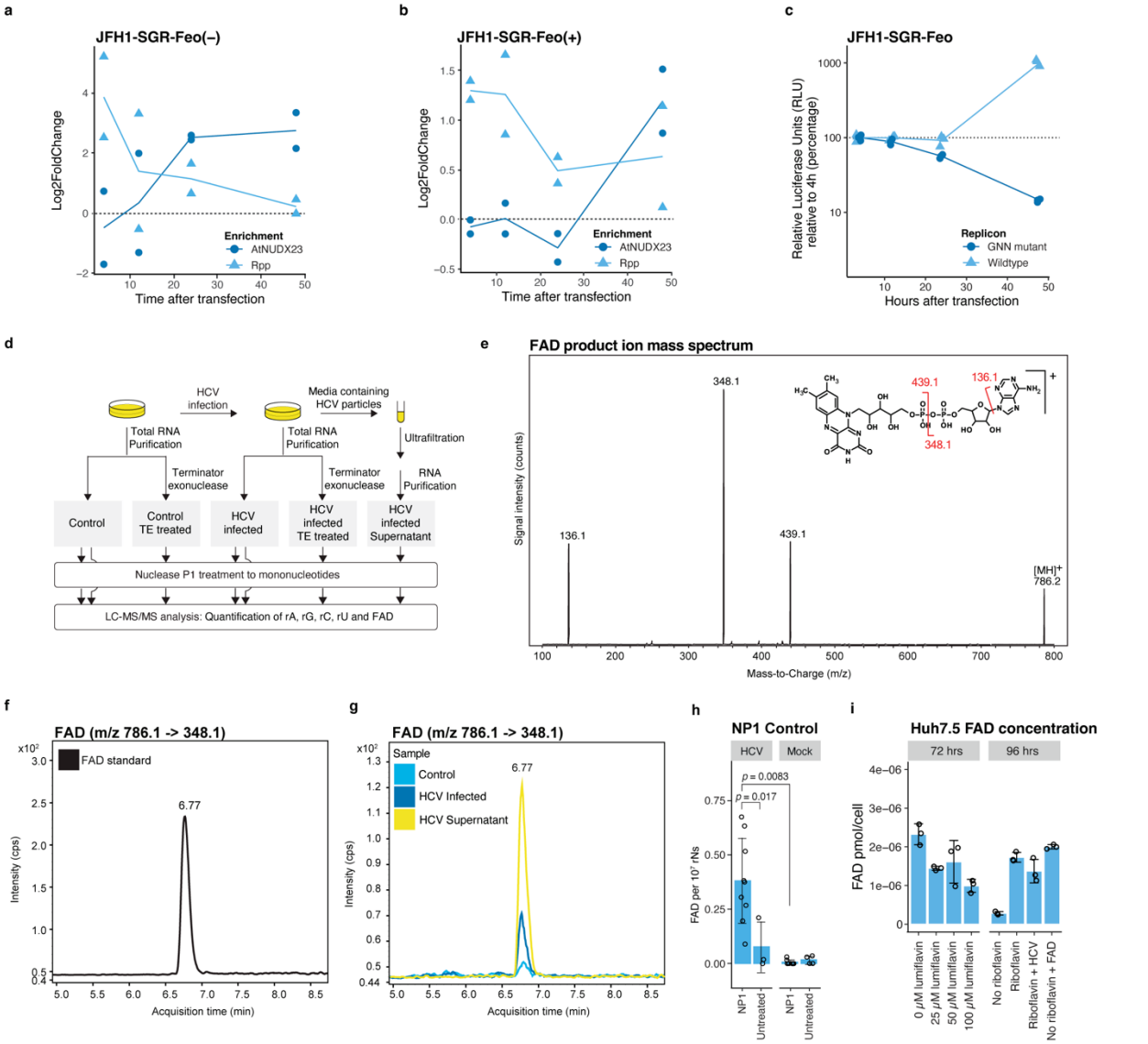

Extended Data Fig.4 | Time course analysis of 5' capping for JFH1-SGR-Feo replicon and LC-MS/MS detection of RNA 5'FAD caps
(a) Enrichment of 5' terminal reads for JFH1-SGR-Feo (–) at the indicated time points. DESeq2 log2(fold change) values were calculated by comparison of enzyme treatment (AtNUDX23 in dark blue and Rpp in light blue) to no enzyme control libraries. The 4 and 12 hrs time points for JFH1-SGR-Feo (–) are associated with uncertainty, because of low counts. (n=2 biological replicates). **(b)** As in (a) but for JFH1-SGR-Feo (+). **(c)** Analysis of viral replication at different time points. Relative luciferase units (RLU) show HCV IRES mediated translation, and replication levels can be deduced by comparing JFH1-SGR-Feo to JFH1-SGR-Feo-GNN (catalytically dead replicon control) at the indicated time points after transfection (n=3 biological replicates). **(d)** Sample preparation for FAD detection using LC-MS/MS. **(e)** FAD product ion mass spectrum. Insert shows the structure of FAD with the detected ions indicated. **(f)** LC-MS/MS chromatogram showing the detection of the FAD control. **(g)** LC-MS/MS chromatogram showing the detection of FAD in a control Huh7.5 mock-infected sample (light blue), intracellular RNA from HCV infected Huh7.5 cells (dark blue) and in HCV particles concentrated from supernatant (yellow). **(h)** LC-MS/MS FAD quantification. FAD concentration based on internal stable isotope-labelled standards for FAD and normalization to ribonucleotide content. RNA was isolated from J6/JFH1 infected or control Huh7.5 cells (mock) and treated with or without Nuclease P1. Due to different lot activities, lower concentration of Nuclease P1 (0.006 U/µg total RNA) was used here, compared to the experiment presented in Fig. 1g (0.12 U/µg total RNA), resulting in lower FAD/rNs ratios. The *p*-values are calculated using one-sided Welch's unequal variances *t*-test. Data are presented as mean +/– SD (n = 9, 3, 9 and 6 from left to right biological replicates). **(i)** Intracellular FAD levels in Huh7.5 cells with and without riboflavin and HCV infection or after lumiflavin treatment. Cells were cultured with or without supplementation of riboflavin (0.4 mg/L) or FAD (10 µM) or were treated with increasing lumiflavin concentrations. HCV indicates infection with J6/JFH1. Fluorescence measurements were used for FAD quantification; shown values for FAD pmol/cell were calculated using a standard curve. Data are presented as mean +/– SD (n=3 biological replicates).

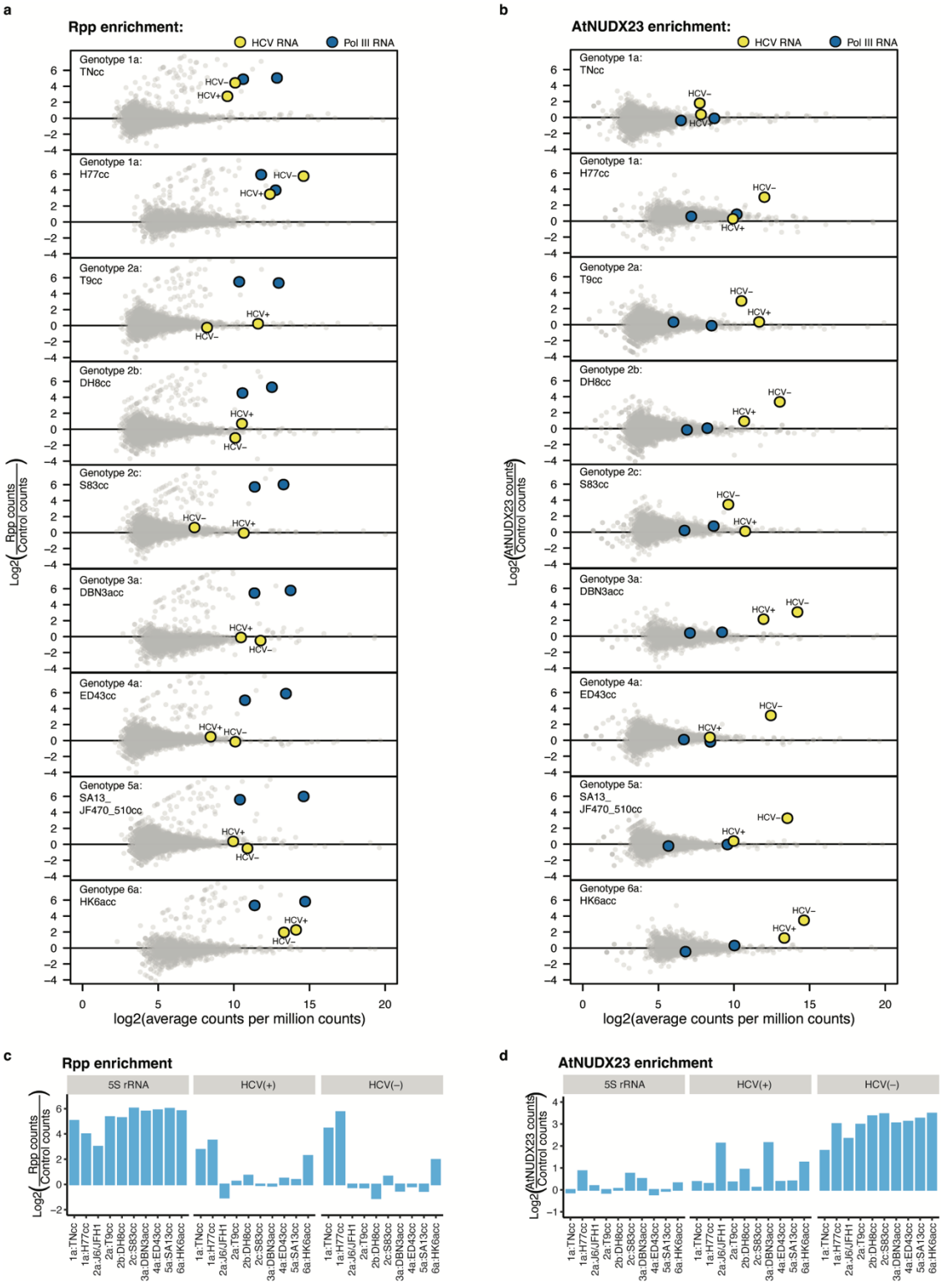

Extended Data Fig.5 | Identification of 5' capping for different HCV strains
CapZyme-seq analysis of RNA isolated from Huh7.5 cells infected with the indicated HCV genotypes/strains. For each genotypes/strains, one Rpp, one AtNUDX23 and none control library was prepared and sequenced. Mean-difference plots show log2 (fold changes) as a function of log2 (average abundance) for reads mapping to the 5' termini of individual RNA molecules. Enrichment with Rpp **(a)** and AtNUDX23 **(b)** was based on comparison of enzyme-treated libraries to no enzyme control libraries. The log2 (fold values) observed for HCV(+), HCV(–) and 5S rRNA (5'ppp) for the different genotypes/strains are summarized in **(c)** for Rpp and **(d)** for AtNUDX23.

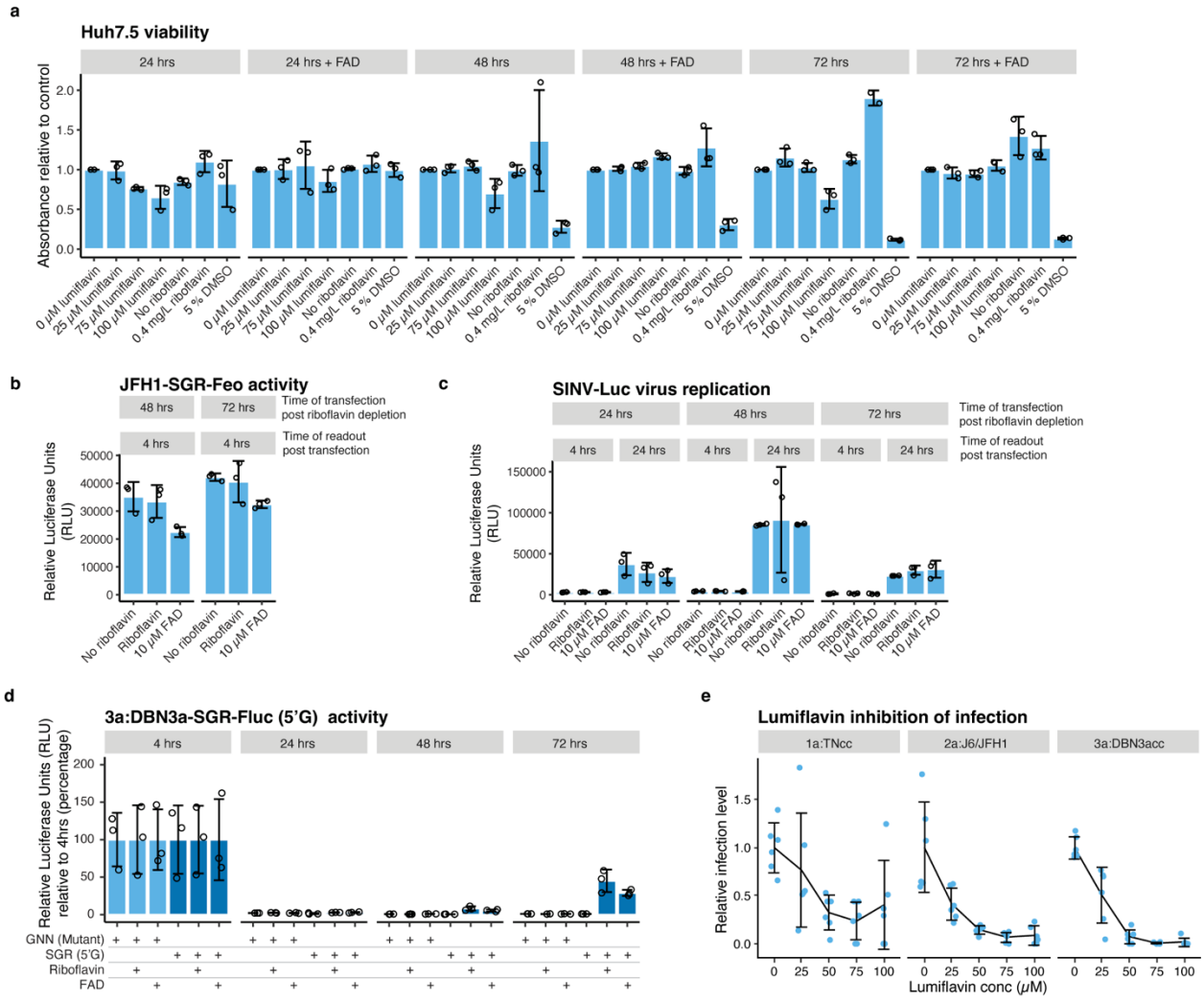

Extended Data Fig.6 | The effect of riboflavin depletion and lumiflavin treatment on cellular viability and HCV genotype-specific dependency on FAD
(a) Cell viability after lumiflavin treatment or riboflavin depletion. **(b)** Measurement of translational activity at 4 hrs after transfection of JFH1-SGR-Feo RNA with and without 0.4 mg/L riboflavin and 10μM FAD. Transfection at several time points after riboflavin depletion was included to exclude that differences in cell viability affected HCV IRES-mediated translation. **(c)** Measurement of Sindbis virus (SINV) replication after transfection of *in vitro* transcribed RNA from infectious SINV Toto-1101/Luc reporter virus with and without 0.4 mg/L riboflavin and 10 μM FAD. Transfection at several time points after riboflavin depletion was included to exclude that differences in cell viability affected SINV replication. **(d)** Replication of DBN3a-SGR(5'G) and GNN (non-replicating mutant) in Huh7.5 cells grown in riboflavin-depleted media. DBN3a-SGR-Fluc(5'G) had partially reverted to 5'A at the 72 hrs time point. Conditions with riboflavin (0.4 mg/L) and FAD (10 μM) included are indicated. Replication was measured in relative luciferase units (RLU) at the indicated time points and quantified relative to 4 hrs. **(e)** Inhibition of HCV infection by lumiflavin. Infection was measured in focus forming units relative to the untreated control obtained after infection with HCV TNcc (1a), J6/JFH1 (2a) or DBN3acc (3a) strains. For all panels, data are presented as mean +/– SD, n=3 biological replicates.

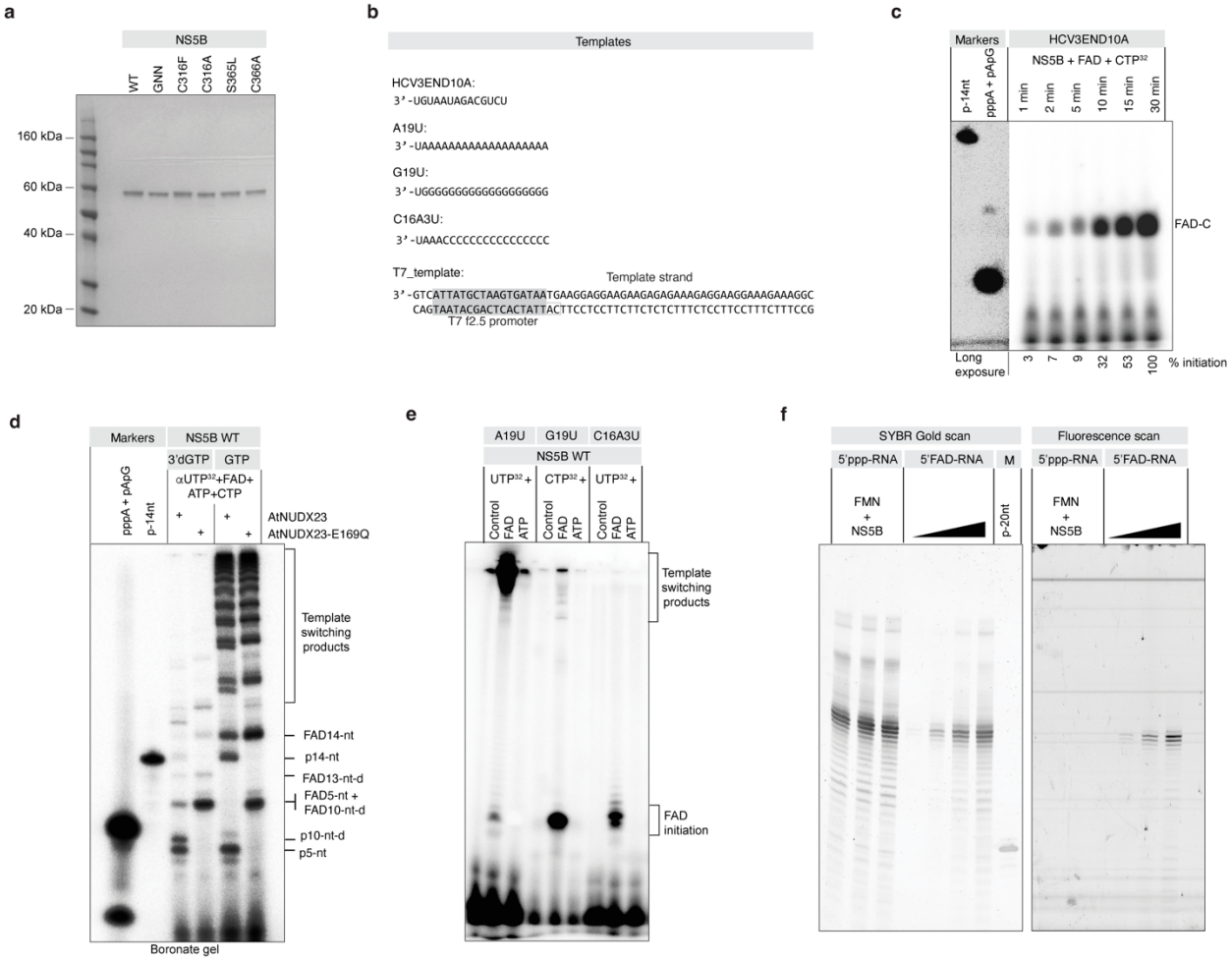

Extended Data Fig.7 | FAD dependent replication initiation by HCV NS5B
(a) Coomassie stained SDS-PAGE of the HCV NS5B WT, GNN, C316F, C316A, S365L and C366A recombinant proteins. **(b)** RNA templates used for *in vitro* replication reactions. **(c)** Time-dependent formation of the initiation product. HCV NS5B polymerase was incubated with HCV3END10A RNA in the presence of FAD and CTP, complemented with α^{32}P-labeled CTP for visualization. Reactions were terminated at the indicated time points. Products were resolved with 18 % denaturing PAGE together with 5' radioactively labelled markers. **(d)** The replication extension products contain FAD. NS5B polymerase was incubated with HCV3END10A RNA in the presence of FAD, ATP, CTP, UTP (complemented with α-32P-labeled UTP) and either GTP or 3'dGTP. After 1 hr incubation, the reactions were treated with AtNUDX23 or AtNUDX23-E169Q. The products were resolved with 18 % denaturing 0.2 % boronate PAGE. The replication reactions subjected to AtNUDX23 or AtNUDX23-E169Q treatment are identical to the α-32P-labeled UTP reactions separated on a regular PAGE gel in main Fig. 3c. The presence of boronate retards FAD-capped RNAs compared to uncapped RNAs due to the relatively stable diol complexes formed between the gel derived boronyl groups and naturally present diols of the RNA 3' end and of FAD. Accordingly, both 5' FAD capping and 3' deoxy termination of extension products will affect migration in the boronate gel. Products were annotated by comparison between the 3'dGTP/GTP conditions, AtNUDX23/AtNUDX23-E169Q conditions and the migration observed on the regular PAGE gel (main Fig. 3c). **(e)** FAD promotes replication initiation on different RNA templates. Indicated RNA templates were incubated with HCV NS5B polymerase. ATP, FAD or control was added as initiating nucleotide. Elongating UTP or CTP nucleotides were supplemented with α^{32}P-labeled UTP or CTP, respectively. The resulting products were resolved with 18 % denaturing PAGE. **(f)** Lack of HCV NS5B mediated post-initiation FAD capping. To exclude that NS5B mediated 5'FAD capping could happen post-initiation on a 5'ppp initiated RNA, 5'ppp RNA was incubated with FMN in the presence of NS5B polymerase. RNA was resolved with 18 % PAGE and visualised by nucleic acid staining (left) and with fluorescent signal indicative of the 5'FAD cap (right). Increasing concentrations of 5'FAD capped RNA generated with T7 polymerase were used as markers on the same gel.

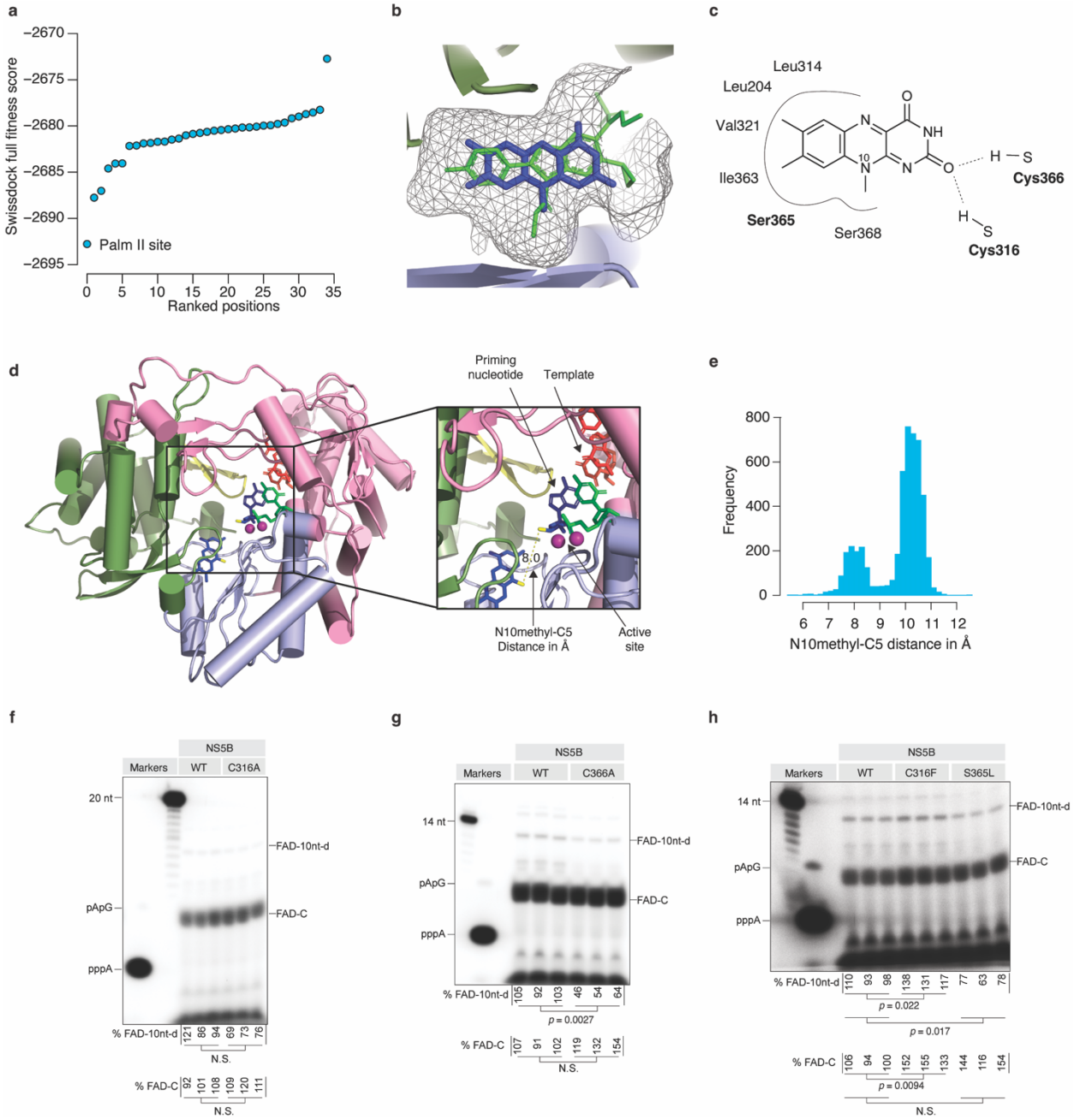

Extended Data Fig.8 | Prediction model of FAD – HCV NS5B interaction
(a) *In silico* docking analysis of FAD into HCV NS5B using SwissDock. Full fitness scores for the top 36 positions obtained by docking of lumiflavin into HCV NS5B are shown. **(b)** Close-up view of the palm II binding pocket demonstrating the overlap between the nesbuvir (green) binding site and the putative binding site of the lumiflavin moiety of FAD (blue). The docking was based on (PDB: 3FQL) with the nesbuvir molecule removed. **(c)** Predicted contacts between NS5B and lumiflavin when docked in the palm II site of NS5B. **(d)** Predicted lumiflavin binding site modelled into the structure of the NS5B primed initiation complex (PDB:4WTM) colored by subdomains: fingers (pink), palm (light blue), thumb (pale green) and beta-loop (yellow). The HCV(+) 3' end sequence was modeled into the position of the template (red). An adenosine (blue) and CMP (green) were modeled into the position of the priming and incoming nucleotides, respectively. The close-up view shows the active site with two localized Mn^{2+} ions in violet. The direct distance between the lumiflavin N10 methyl and the ribose C5 is indicated. **(e)** Observed FAD N10 methyl-C5 distances from 4,928 crystal structures of proteins containing a FAD cofactor. **(f-h)** Triplicate analysis (independent replicates) of *de novo* initiation with FAD for the indicated NS5B mutants using the HCV3END10A template with the FAD extension and initiation signal quantified below the gels. The *p*-values are calculated using two-sided Welch's unequal variances *t*-test. N.S. equals *p*-val > 0.05.

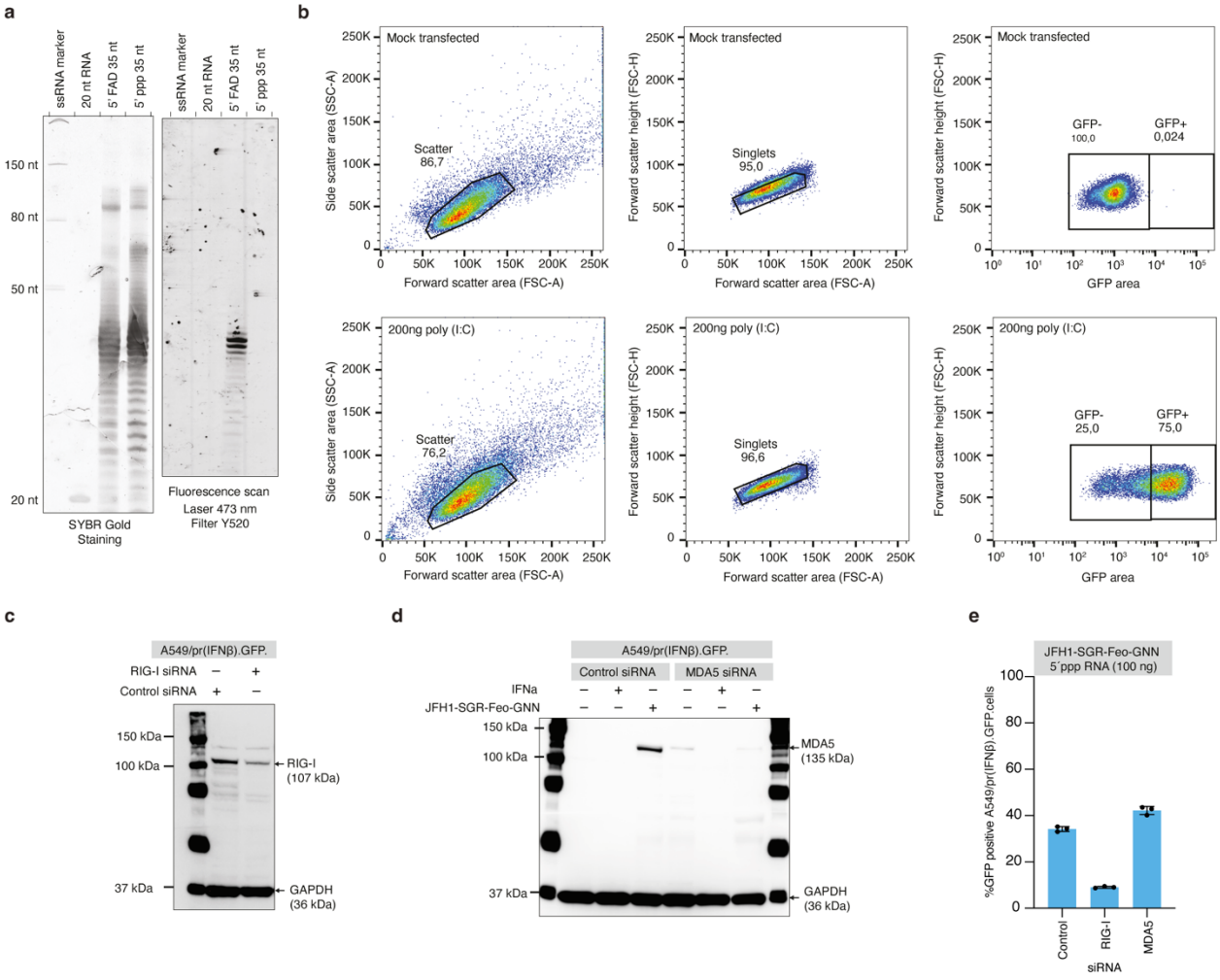

Extended Data Fig.9 | Extended data relating to RNA stimulation of innate immune responses.
(a) Analysis of the *in vitro* transcribed RNAs used in cell-intrinsic innate immune recognition experiments (main Fig. 4c-g). RNA was resolved with 18 % PAGE and visualised by nucleic acid staining (left) or with fluorescent signal from the 5'FAD cap (right). **(b)** Gating strategy for flow cytometry experiments. Mock- and poly (I:C) transfected A549/pr(IFNβ).GFP reporter cells were used to set gates. Live cells were SSC-A:FSC-A gated, followed by FSC-H:FSC-A gating to select single cells. Single cells were then GFP(–) or GFP(+) gated. **(c)** Immunoblot for RIG-I after control or *RIGI* siRNA mediated knock-down in A549/pr(IFNβ).GFP reporter cells. The RIG-I specific band is indicated. **(d)** Immunoblot for MDA5 after control or *MDA5* siRNA mediated knock-down in A549/pr(IFNβ).GFP reporter cells and induction of MDA5 expression by transfection with 5´ppp JFH1-SGR-Feo-GNN RNA. 50 IU/mL IFN-α 2a, is shown for comparison; this concentration was too low to induce MDA5 expression at the shown exposure level. **(e)** Analysis of innate immune activation upon transfection of JFH1-SGR-Feo-GNN replicon RNA into A549/pr(IFNβ).GFP cells after knock-down of RIG-I or MDA5. Data are presented as mean +/– SD, n=3 biological replicates.

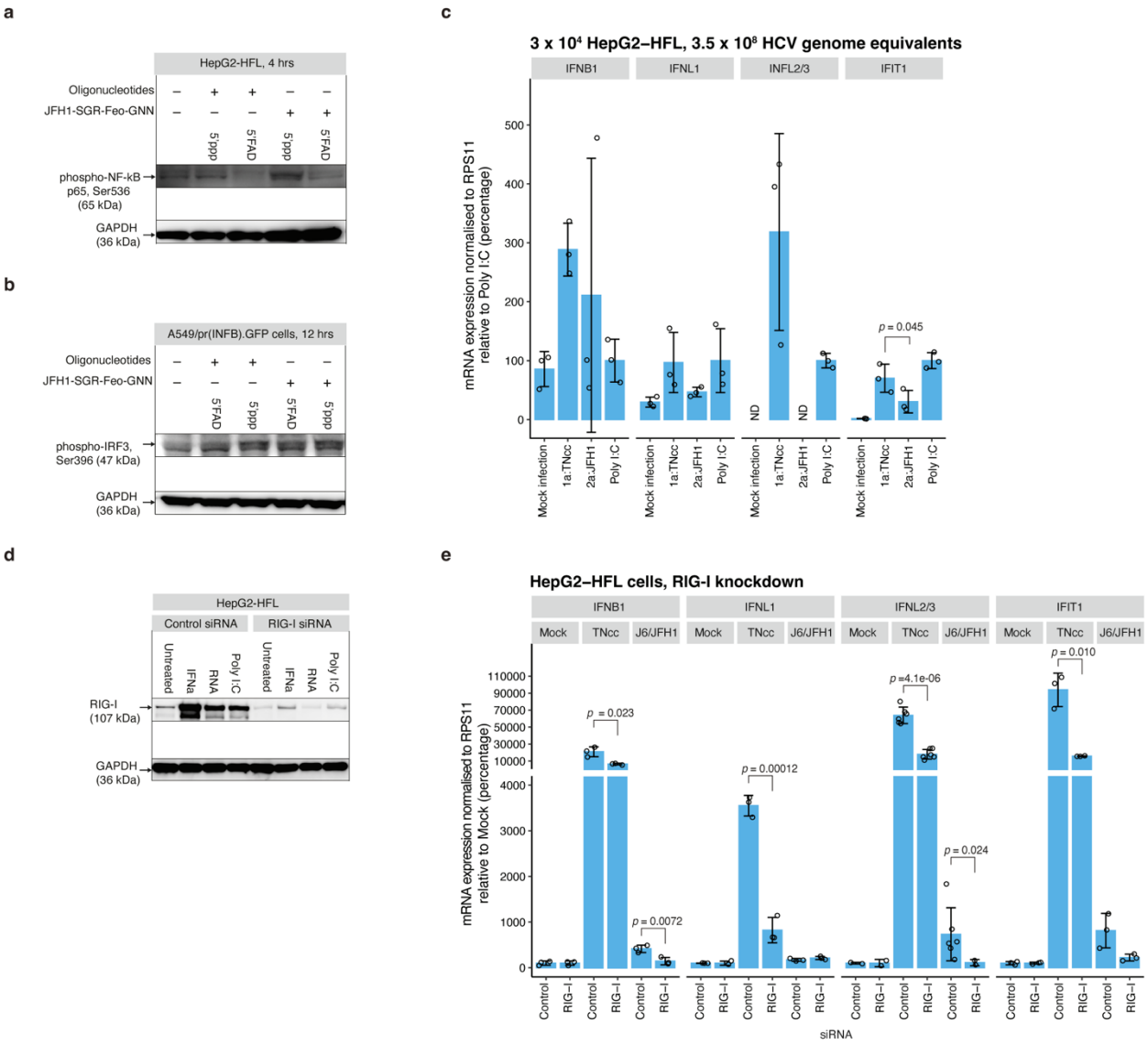

Extended Data Fig.10 | Extended data relating to RNA stimulation of innate immune responses.
(a) Immunoblot for phosphorylated NF-κB subunit p65 in HepG2-HFL cells 4 hrs after stimulation with 5'ppp or 5'FAD as indicated. **(b)** Immunoblot for phosphorylated IRF3 in A549/pr(IFNβ).GFP cells 12 hrs after stimulation with 5'ppp or 5'FAD as indicated. The upper band, consistent with the size of p-IRF3 appears only after stimulation. Note the different loading order compared to panel (a). **(c)** mRNA expression levels for *IFNB1*, *IFNL1*, *IFNL2/3* and *IFIT1* 18 hrs post infection of HepG2-HFL cells with equal RNA titers of indicated HCV strains shown relative to polyI:C induced levels. Data are presented as mean +/– SD (n=3 biological replicates). ND: Not detected. **(d)** Immunoblot for RIG-I after control or *RIGI* siRNA mediated knock-down in HepG2-HFL cells and induction of RIG-I expression by transfection of 100 ng *in vitro* transcribed 5´ppp J6/JFH1 RNA, 100 ng Poly I:C or treatment with 500 U/mL IFN-α 2a. **(e)** mRNA expression levels for *IFNB1*, *IFNL1*, *IFNL2/3* and *IFIT1* 18 hrs post infection of HepG2-HFL cells with indicated HCV strains shown relative to levels obtained for Mock infected control siRNA treated cells. Data are presented as mean +/– SD (n=3 biological replicates). Prior to infection, cells were transfected with control siRNA or *RIGI* targeting siRNA. The *p*-values in (c) and (e) are calculated using one-sided Welch's unequal variances *t*-test by comparing to the mock infection samples.